



## FULL LENGTH ARTICLE

# Lack of interferon regulatory factor 3 leads to anxiety/depression-like behaviors through disrupting the balance of neuronal excitation and inhibition in mice



Junjie Li, Yayan Pang, Yehong Du, Lei Xia, Mulan Chen, Yepeng Fan, Zhifang Dong\*

*Pediatric Research Institute, Ministry of Education Key Laboratory of Child Development and Disorders, National Clinical Research Center for Child Health and Disorders, China International Science and Technology Cooperation Base of Child Development and Critical Disorders, Chongqing Key Laboratory of Translational Medical Research in Cognitive Development and Learning and Memory Disorders, Children's Hospital of Chongqing Medical University, Chongqing 400014, China*

Received 8 February 2022; received in revised form 20 April 2022; accepted 5 May 2022  
Available online 19 May 2022

**KEYWORDS**

Anxiety;  
Depression;  
Hippocampus;  
IRF3;  
Medial prefrontal cortex;  
Synaptic transmission

**Abstract** Disrupting the balance of neuronal excitation and inhibition (E/I) is an important pathogenic mechanism of anxiety and depression. Interferon regulatory factor 3 (IRF3) plays a key role in the innate immune response, and activation of IRF3 triggers the expression of type I interferons and downstream interferon-stimulated genes, which are associated with anxiety and depression. However, whether IRF3 participates in the pathogenesis of anxiety/depression by regulating E/I balance remains poorly understood. Here, we reported that global knockout (KO) of IRF3 (*IRF3*<sup>-/-</sup>) significantly increased anxiety/depression-like behaviors, but did not affect normal spatial learning and memory. Compared with wild type (WT) control mice, the E/I balance was disrupted, as reflected by enhanced glutamatergic transmission and decreased GABAergic transmission in the neurons of hippocampal CA1 and medial prefrontal cortex (mPFC) in *IRF3*-KO mice. Importantly, genetic rescue of IRF3 expression by adeno-associated virus (AAV) was sufficient to alleviate anxiety/depression-like behaviors and restore the neuronal E/I balance in *IRF3*-KO mice. Taken together, our results indicate that IRF3 is critical in maintaining neuronal E/I balance, thereby playing an essential role in ensuring emotional stability.

© 2022 The Authors. Publishing services by Elsevier B.V. on behalf of KeAi Communications Co., Ltd. This is an open access article under the CC BY-NC-ND license (<http://creativecommons.org/licenses/by-nc-nd/4.0/>).

\* Corresponding author.

E-mail address: [zfdong@cqmu.edu.cn](mailto:zfdong@cqmu.edu.cn) (Z. Dong).

Peer review under responsibility of Chongqing Medical University.

<https://doi.org/10.1016/j.gendis.2022.05.003>

2352-3042/© 2022 The Authors. Publishing services by Elsevier B.V. on behalf of KeAi Communications Co., Ltd. This is an open access article under the CC BY-NC-ND license (<http://creativecommons.org/licenses/by-nc-nd/4.0/>).

## Introduction

Anxiety and depression are the most common comorbid mood disorders with high morbidity, mortality and disability rates, which cause the enormous burden of economic and spirit on their families and society.<sup>1–3</sup> So far, chemical drugs and psychotherapy are the main treatments for anxiety and depression comorbidities, but the treatment is usually inadequate and easy to relapse.<sup>4,5</sup> Therefore, it is vital to further explore the pathogenesis of anxiety and depression comorbidity in order to assist in diagnosis and treatment. Increasing evidence indicates that the balance of neuronal excitation and inhibition (E/I) is essential for maintaining normal brain function.<sup>6,7</sup> E/I imbalance will lead to a variety of mental disorders, including anxiety, depression and schizophrenia, etc.<sup>8,9</sup> Given that the hippocampus and medial prefrontal cortex (mPFC) have a large number of excitatory and inhibitory neurons, which play a crucial role in regulating brain E/I balance,<sup>10</sup> the hippocampus and mPFC play important roles in emotional regulation, especially for anxiety and depression.<sup>11–13</sup> Understanding the neural mechanisms that govern the balance of neuronal E/I in the hippocampus and mPFC has an important role in the diagnosis and treatment of hippocampus/mPFC-related anxiety and depression comorbid disorders.

Interferon regulatory factor 3 (IRF3) is a member of the IRF family with 427 amino acids and a molecular weight of about 55 kD that is expressed in all tissues and cells.<sup>14,15</sup> IRF3 is a central component of the innate immune system. Activation of *IRF3* triggers the production of type I interferons (*IFN- $\alpha$*  and *IFN- $\beta$* ) and downstream interferon-stimulated genes.<sup>16</sup> Growing evidence suggests that IRFs, including IRF3, are essential for maintaining physical health in mammals and humans, and that their abnormal expression and regulation lead to various diseases.<sup>17–19</sup> Although IRF3 has been widely studied in anti-infective immunity,<sup>20–23</sup> tumor immunity,<sup>24–26</sup> stroke<sup>27,28</sup> and metabolism,<sup>29–32</sup> much less is known about the role of IRF3 in psychological disorders such as anxiety and depression. Recent studies have shown that the activation of IRF3/*IFN- $\beta$*  signaling pathway is able to suppress neuronal excitability in the hippocampus during seizures.<sup>33</sup> Therefore, we hypothesize that IRF3 signaling may be involved in the development of psychological disorders such as anxiety and depression by regulating the neuronal E/I balance in the hippocampus and/or other regions of the brain. In the present study, we investigated this hypothesis using a combination of electrophysiological and behavioral assessments in *IRF3*-deficient (*IRF3*<sup>-/-</sup>) mice.

## Materials and methods

### Animals

The *IRF3*<sup>-/-</sup> mice with C57BL/6J background have been described previously<sup>34</sup> and were gifts from Professor Sen Lin (Army Medical University, Chongqing, China). Heterozygotes (*IRF3*<sup>+/-</sup>) crossed to generate *IRF3* knockout (KO) and wild-type (WT) littermates for experiments. All animals were housed in plastic cages with unlimited access to food and water and maintained in a temperature-controlled

colony room (21 °C) under a cycle of 12-h light/12-h dark (7:00 am–7:00 pm). All transgenic mice were genotyped by PCR with reverse transcriptase using mouse tail-tip DNA and common primers (5'-GAACCTCGGAGTTATCCCGAAGG-3'), WT primers (5'-GTTTGAGTTATCCCTGCACTTGGG-3') for 350 bp and mutant primers (5'-TCGTGCTTTACGC-TATCGCCGCTCCCGATT-3') for 450 bp (Fig. 1A). Further protein expression of IRF3 was determined by Western blotting (Fig. 1B). Anti-IRF3 antibody (4302S, 1:1000) was purchased from Cell Signaling Technology and anti-GAPDH antibody (ARG10112, 1:5000) was from Arigo Bio-laboratories Corp. All procedures were performed in accordance with the Chongqing Science and Technology Commission guidelines and approved by the Animal Ethics Committee of Children's Hospital of Chongqing Medical University (Approval number: CHCMU-IACUC20210114017). All efforts were made to minimize animal discomfort and to reduce the number of animals used.

### Adeno-associated virus (AAV) microinjection

To rescue the expression of IRF3 in the brain, AAV9 carrying IRF3-EGFP-3FLAG (AAV<sub>IRF3</sub>) or its control (AAV<sub>EGFP</sub>) were constructed by Genechem Technology (Shanghai, China). The titer of each virus was  $5 \times 10^{12}$  TU/mL. As previously described,<sup>35</sup> 6-week old mice were deeply anesthetized with pentobarbital sodium and fixed in a stereotaxic apparatus (RWD Life Science Co., Shenzhen, China). A hole was drilled and 2  $\mu$ L of AAV was microinjected into the lateral cerebral ventricle (-0.5 mm posterior, 1.0 mm lateral and -2.5 mm ventral relative to bregma). Electrophysiological and behavioral experiments were performed 6 weeks after AAV microinjection.

### Open field test

The open field arena consisted of a clear plastic box (42 cm  $\times$  42 cm  $\times$  42 cm) was used to assess anxiety-like behavior. Mice were placed in the center of the open field to freely explore for 10 min. The time and the number of entries in the center zone were recorded using the ANY-maze tracking system (Stoelting, USA). The chamber was cleaned with 75% ethanol and water between each trial to avoid any odor from the previous mouse.

### Elevated plus maze test

The maze consisted of two open arms and two closed arms (15-cm-tall walls on the closed arms) arranged at right angles (each arm 30 cm). During the test, mice were placed in the central zone (5 cm  $\times$  5 cm) that was elevated 70 cm above the floor, and allowed to explore the apparatus for 5 min. The number of entries into the open arms and the time spent in the open arms were recorded by ANY-maze tracking system (Stoelting, USA). All test arms were cleaned with 75% alcohol and water between each mouse.

### Tail suspension test

To evaluate depressive-like behavior, mice were individually suspended by their tail using medical tapes on the

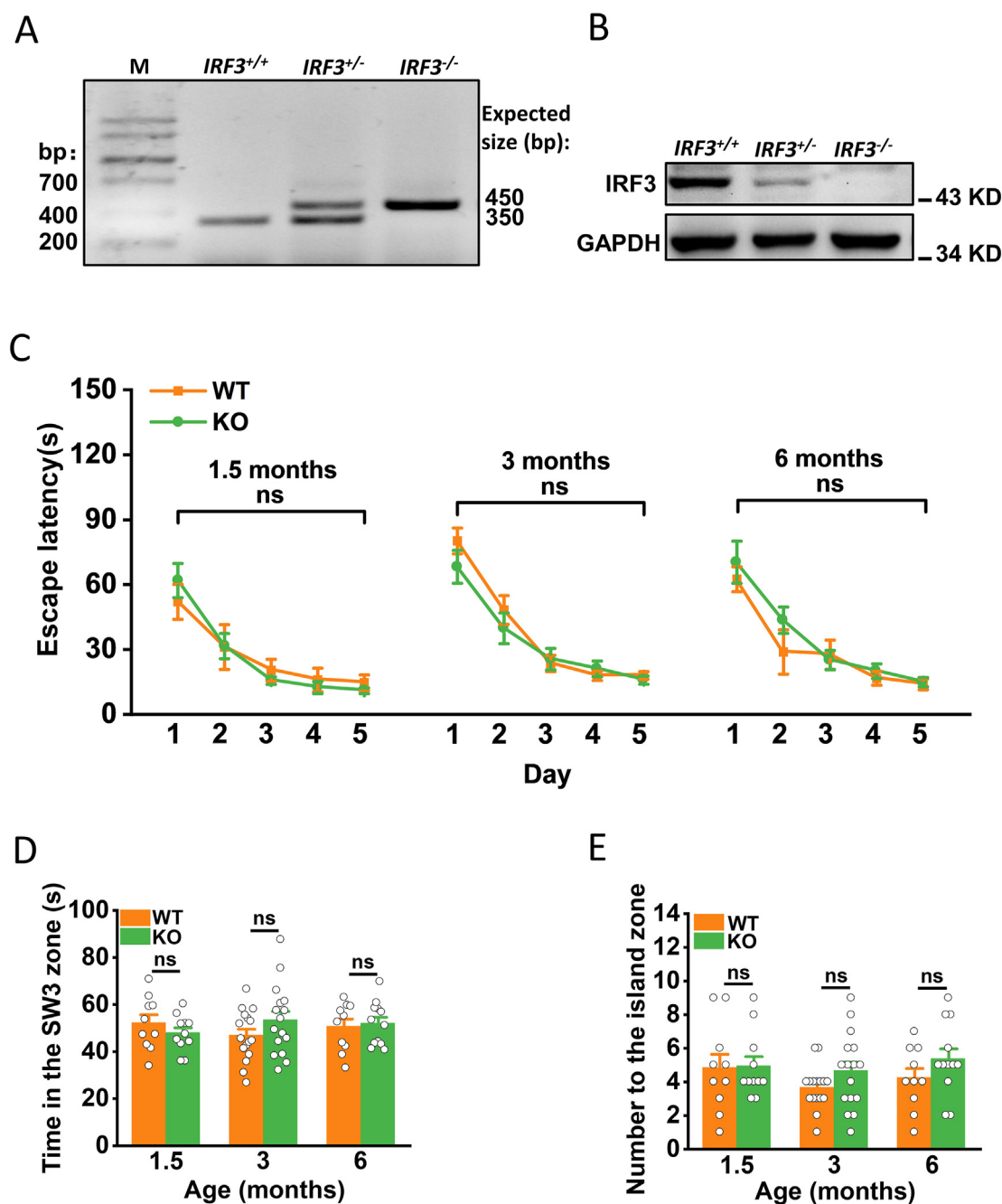


**Figure 1** *IRF3*-KO mice have no effect on spatial learning and memory. (A, B) *IRF3* KO mice were verified by PCR (A) and Western blotting (B). (C) The escape latency to the hidden platform during the Morris water maze training ( $n = 10\text{--}16$  per group). Repeated measures ANOVA: 1.5 m,  $F(1,19) = 76.335$ ,  $P = 0.955$ ; 3 m,  $F(1,30) = 76.335$ ,  $P = 0.426$ ; 6 m,  $F(1,20) = 256.528$ ,  $P = 0.368$ . (D) The time spent in the target quadrant during the Morris water maze test. Unpaired Student's  $t$ -test: 1.5 m,  $t = 2.284$ ,  $P = 0.321$ ; 3 m,  $t = 1.291$ ,  $P = 0.170$ ; 6 m,  $t = 0.308$ ,  $P = 0.760$ . (E) The number of entries to the platform zone during the Morris water maze test. Unpaired Student's  $t$ -test: 1.5 m,  $t = 0.617$ ,  $P = 0.916$ ; 3 m,  $t = 5.366$ ,  $P = 0.131$ ; 6 m,  $t = 0.099$ ,  $P = 0.212$ . Data are expressed as mean  $\pm$  SEM. \* $P < 0.05$ , \*\* $P < 0.01$ , \*\*\* $P < 0.001$ ; ns, no significant difference.

metal hook of horizontal rails (45 cm above floor) and recorded for 6 min by ANY-maze tracking system (Stoelting, USA). Latency to immobility and the total immobility time during the last 5 min of the 6 min were recorded by two independent observers who were blind to the animals grouping.

#### Forced swimming test

In the forced swim test, mice were placed in a transparent cylindrical tanks (12 cm diameter, 30 cm height) filled with 22–24 °C water and videotaped for 10 min using ANY-maze tracking system (Stoelting, USA). Latency to immobility and

total immobility time were recorded by two blinded observers to measure depression-like behavior. After the test, animals were dried with a paper towel and then returned to their home cage.

### Morris water maze test

The Morris water maze test was typically performed to evaluate spatial learning and memory capacity in mice as described previously.<sup>36,37</sup> The maze consisted of a cylindrical nonrust steel pool (diameter: 150 cm, height: 60 cm) filled with opaque water ( $23 \pm 1$  °C) made of non-toxic white paint. The pool was localized in a quiet room with 3 visible large size cues. The experimental process lasted for 7 days. On the first day, animals were placed in the pool without a hidden circular platform and allowed to adapt to the pool for 120 s. Spatial learning tasks were conducted over the next five days and each mouse was trained 4 trials per day. The mouse was placed into four randomly quadrants (NE, NW, SW, and SE) and allowed to find the submerged platform (7.5 cm in diameter, located 1.5 cm below the opaque water) in 120 s. If the animal did not find the platform at the end of the training, it was guided to the platform to remain 20 s. Twenty-four hours after the final training trial, a 120-sec probe test was performed without the hidden platform to assess the memory retrieval. All trials were recorded by using Any-maze tracking system (Stoelting, USA).

### Western blotting

Mice were euthanized with over dose of urethane (1.5 g/kg, i.p.) and rapidly decapitated after behavioral tests. Tissue samples (hippocampus and frontal cortex) were immediately collected for Western blotting. For total protein extraction, brain tissue was homogenized in 0.15 mL ice-cold RIPA buffer with a cocktail protease inhibitor (Complete, Roche) and the lysates were centrifuged at 12,000 rpm at 4 °C for 15 min to collect the supernatants. Protein concentrations were measured using the BCA assay (Thermo Fisher Scientific, USA). Equivalent protein (30 µg) was denatured at 98 °C in 5× loading buffer for 5 min. Protein samples were loaded on 10% SDS-PAGE gel for approximately 100 min, and then transferred onto PVDF membrane. The membranes were blocked using 5% non-fat milk in TBST for 60 min at room temperature, and then incubated with primary antibodies overnight in 4 °C refrigerator. Subsequently, all membranes were washed three times with TBST for 5 min each time and incubated with an HRP-conjugated secondary antibody (1:3000, PerkinElmer) at room temperature for 1 h. The protein was detected with the Bio-Rad (Bio-Rad, USA) Imager using ECL Western blotting substrate (Pierce, Waltham, USA).

### Immunofluorescence staining

Immunofluorescence staining was used to detect the effects of viral infection 1.5 months after AAV injection. In brief, mice were euthanized with over dose of urethane (1.5 g/kg, i.p.) and transcardially perfused with 20 mL of 4% paraformaldehyde (PFA) before being decapitated. Brains

were rapidly dissected out after decapitation and post-fixed in 4% PFA overnight, then dehydrated in 20% and 30% sucrose for 24 h respectively, and serially sectioned into 30 µm-thick coronal sections. Frozen sections were washed in phosphate-buffered saline (PBS) and attached to glass slides, which were then coated with anti-fade mounting medium with DAPI and covered with coverslips. The immunofluorescent signal was monitored on a laser scanning confocal microscope (Nikon, Japan) at wavelengths of 488 nm (green, EGFP) and 405 nm (blue, DAPI).

### Electrophysiological recordings

For slice preparation,<sup>38,39</sup> the mice (16-week old) were deeply anesthetized via urethane (1.5 g/kg, i.p.) and transcardially perfused with 15 mL of NMDG based ice-cold cutting solution containing 92 mM NMDG, 2.5 mM KCl, 1.25 mM NaH<sub>2</sub>PO<sub>4</sub>·H<sub>2</sub>O, 30 mM NaHCO<sub>3</sub>, 20 mM HEPES, 25 mM D-glucose, 5 mM Na-ascorbate, 3 mM Na-pyruvate, 2 mM Thiourea, 12 mM NAC, 0.5 mM CaCl<sub>2</sub> and 10 mM MgCl<sub>2</sub> (with osmolarity of 295–305 mOsm/l). After decapitation, the brain was rapidly removed and submerged in ice cold NMDG solution oxygenated with 95% O<sub>2</sub> and 5% CO<sub>2</sub>. Acute coronal slices (300–400 µm) were cut on a vibratome (VT1200S, Leica Microsystems, Germany) and then incubated in carbogen (95% CO<sub>2</sub>/5% O<sub>2</sub>) NMDG buffer (35 °C) to recover for 15 min. After that, all slices were transferred into a braincubator filled with incubation buffer containing 92 mM NaCl, 2.5 mM KCl, 1.25 mM NaH<sub>2</sub>PO<sub>4</sub>·H<sub>2</sub>O, 30 mM NaHCO<sub>3</sub>, 20 mM HEPES, 25 mM D-glucose, 5 mM Na-ascorbate, 3 mM Na-pyruvate, 2 mM Thiourea, 12 mM NAC, 2 mM CaCl<sub>2</sub> and 2 mM MgCl<sub>2</sub> (pH 7.4, 295–305 mOsm/L) for 1 h at room temperature (23–25 °C) prior to recording. Then the slices were transferred out by a dropper to the flow chamber filled with bubbled recording solution including 120 mM NaCl, 2.5 mM KCl, 1.25 mM NaH<sub>2</sub>PO<sub>4</sub>·H<sub>2</sub>O, 24 mM NaHCO<sub>3</sub>, 5 mM HEPES, 12.5 mM D-glucose, 2 mM CaCl<sub>2</sub> and 2 mM MgCl<sub>2</sub> at pH 7.4, 295–305 mOsm/L.

Whole cell patch-clamp recordings were performed at room temperature in hippocampal CA1 and medial prefrontal cortex (mPFC) neurons using a HEKA EPC10 amplifier (HEKA, Germany) and PatchMaster software (filtered at 3 kHz and sampled at 10 kHz). Patch pipettes were pulled from 1.5-mm diameter borosilicate glass capillaries on a horizontal micropipette puller (P-97, Sutter Instruments). For recordings of action potential (APs),<sup>39</sup> the internal solution contained (in mM): 117 K-Gluconate, 4 NaCl, 13 KCl, 10 HEPES, 0.1 EGTA, 2 Mg-ATP, 0.4 Na-GTP and 0.07 CaCl<sub>2</sub>, pH 7.2–7.3 with KOH, 295–305 mOsm/L. AP (–70 mV holding potential) spikes were elicited by injecting rectangular current (360 ms duration currents, 0–180 pA with 20 pA step increment). Resting membrane potential, APs threshold and APs firing rate were analyzed with Clampfit 10.7 software (Molecular Devices). For the miniature responses, the mEPSC and mIPSC were recorded at holding potential of –70 mV. For mIPSC recordings, synaptic blockers (20 µM CNQX, 50 µM AP5 and 0.5 µM TTX) were added into the recording buffer. Borosilicate glass electrodes (4–6 MΩ) were filled with intracellular solutions consisting of (in mM): 140 CsCl, 0.15 CaCl<sub>2</sub>, 10 HEPES, 4.25 MgCl<sub>2</sub>, 0.5 EGTA and 4 K-ATP, pH 7.2–7.3 with CsOH,

295–305 mOsm/L. To record mEPSC, PTX (100  $\mu$ M) and TTX (0.5  $\mu$ M) were added to the extracellular solution and the internal electrode solution contained (in mM): 120 CsMeSO<sub>3</sub>, 15 CsCl, 0.2 EGTA, 10 HEPES, 2 ATP-Mg, 8 NaCl, 2 QX-314, 10 TEA-Cl and 0.3 Na-GTP, pH 7.2–7.3 with CsOH, 295–305 mOsm/L. The frequency and amplitude of mEPSC and mIPSC were quantified by Mini Analysis Program 6.0.3 (Synaptosoft Inc., Decatur, GA).

### Statistical analysis

All data are presented as mean  $\pm$  SEM. The two-tailed Student's *t*-test was used to evaluate statistical significance between two groups. The data of multiple groups were analyzed by one-way ANOVA or Repeated measures ANOVA followed by Least Significant Difference (LSD) post hoc test. Statistical significance was set as at \**P* < 0.05, \*\**P* < 0.01, \*\*\**P* < 0.001; ns, no significant difference.

## Results

### IRF3-KO mice exhibit normal spatial learning and memory

Prior to behavioral experiments, mice were genotyped by PCR (Fig. 1A) and Western blotting (Fig. 1B). The results showed that the *IRF3*-KO (*IRF3*<sup>-/-</sup>) mouse model was successfully developed. Next, the Morris water maze test was performed in 1.5-, 3- and 6-month-old mice to assess the effect of *IRF3* on spatial learning and memory. The results showed that no any significant difference in escape latency was observed during spatial learning between WT and *IRF3*-KO mice (1.5-month: *P* = 0.955; 3-month: *P* = 0.426; 6-month: *P* = 0.368; Fig. 1C). Further probe test showed that *IRF3*-KO had no effect on spatial memory retrieval, as reflected by no any difference in the time spent in the target quadrant (1.5-month: WT, *n* = 10, KO, *n* = 11, *P* = 0.321; 3-month: WT, *n* = 16, KO, *n* = 16, *P* = 0.170; 6-month: WT, *n* = 10, KO, *n* = 12, *P* = 0.760; Fig. 1D) and the number of platform crossings (1.5-month: *P* = 0.916; 3-month: *P* = 0.131; 6-month: *P* = 0.212; Fig. 1E) between WT and KO mice. These results suggest that *IRF3*-KO does not affect spatial learning and memory.

### IRF3-KO mice exhibit anxiety/depression-like behaviors

Clinical studies have reported that *IRF3* might be associated with anxiety and depression in patients.<sup>40,41</sup> To determine the role of *IRF3* in anxiety/depression-like behaviors, the open field test, elevated plus maze test, tail suspension test and forced swimming test were introduced to measure anxiety/depression-like behaviors in *IRF3*-KO mice. In the open field task, 1.5-month *IRF3*-KO mice did not show any anxiety-like behavior (WT, *n* = 10, KO, *n* = 11, *P* = 0.159 for the time in the center zone, *P* = 0.416 for the number to the center zone; Fig. 2A–C). However, the *IRF3*-KO mice at 3-month and 6-month old displayed obvious anxiety-like behavior, as reflected by a significant decrease in the time in the center zone (3-month: WT, *n* = 10, KO, *n* = 10,

*P* = 0.001; 6-month: WT, *n* = 11, KO, *n* = 13, *P* < 0.001; Fig. 2A, B) and the number to the center zone (*P* < 0.001 for 3-month; *P* < 0.001 for 6-month; Fig. 2A, C). To further confirm the anxiety-like behavior in *IRF3*-KO mice, we next conducted the elevated plus maze test. The results showed that *IRF3*-KO mice did not exhibit anxiety-like behavior at 1.5-month old (WT, *n* = 10, KO, *n* = 11, *P* = 0.921 for the time in the open arm, *P* = 0.184 for the number to the open arm; Fig. 2D–F). Similar to that in the open field test, the *IRF3*-KO mice at 3-month and 6-month old spent much less time in the open arm (3-month: WT, *n* = 18, KO, *n* = 19, *P* < 0.001; 6-month: WT, *n* = 11, KO, *n* = 13, *P* = 0.009; Fig. 2D, E) and significantly decreased entries to the open arm (*P* < 0.001 for 3-month; *P* = 0.004 for 6-month; Fig. 2D, F) compared to WT during elevated plus maze test.

Next, using tail suspension and forced swimming paradigms, we tested the influence of *IRF3* on depression-like behavior in *IRF3*-KO mice. The results showed that the total immobility time (WT, *n* = 8, KO, *n* = 8, *P* = 0.535; Fig. 2G) and the latency to immobility (*P* = 0.512; Fig. 2H) remained unchanged in *IRF3*-KO mice at 1.5-month-old, compared to WT, during tail suspension test. The *IRF3*-KO mice at 3-month and 6-month-old displayed obvious depression-like behavior compared to WT, because the total immobility time (3-month: WT, *n* = 16, KO, *n* = 17, *P* = 0.003; 6-month: WT, *n* = 10, KO, *n* = 12, *P* = 0.002; Fig. 2G) was significantly increased while the latency to immobility (*P* = 0.008; Fig. 2H) was markedly decreased. Similar to that in the tail suspension test, *IRF3*-KO mice did not exhibit depression-like behavior at 1.5-month-old during forced swimming test (WT, *n* = 8, KO, *n* = 8, *P* = 0.429 for the total immobile time, *P* = 0.074 for the latency to immobility; Fig. 2I, J). As expected, the *IRF3*-KO mice at 3-month and 6-month old displayed obvious depression-like behavior compared to WT, as reflected by a significant increase in the total immobility time (3-month: WT, *n* = 18, KO, *n* = 16, *P* = 0.007; 6-month: WT, *n* = 10, KO, *n* = 12, *P* < 0.001; Fig. 2I, J) and decrease in the latency to immobility (*P* = 0.267 for 3-month; *P* = 0.004 for 6-month; Fig. 2I, J). Together, these results suggest that *IRF3* deficiency causes age-dependent anxiety/depression-like behaviors in mouse models.

### Expression of IRF3 reverses anxiety/depression-like behaviors in IRF3-KO mice

To determine whether the anxiety/depression-like behaviors in *IRF3*-KO mice are attributable to *IRF3* deficiency, we overexpressed functional *IRF3* in the brain at 1.5 months of age by intracerebroventricular (i.c.v.) microinjection of adeno-associated viruses carrying *IRF3* (AAV<sub>IRF3</sub>), and examined its ability to rescue the behavioral phenotypes in the *IRF3*-KO mice at 3-month-old. Immunofluorescence assay showed that i.c.v. microinjection of AAV<sub>IRF3</sub> could effectively infect the neurons in the mPFC and hippocampus, and the Western blotting results indicated that AAV<sub>IRF3</sub> succeeded in restoring the expression of *IRF3* in *IRF3*-KO mice (Fig. 3A, B). We further found that there was a significant increase in the time (WT, *n* = 17; KO + AAV<sub>EGFP</sub>, *n* = 11, *P* < 0.001 vs. KO + AAV<sub>EGFP</sub>; KO + AAV<sub>IRF3</sub>, *n* = 12, *P* < 0.001 vs. KO + AAV<sub>EGFP</sub>; Fig. 3C, D) and number

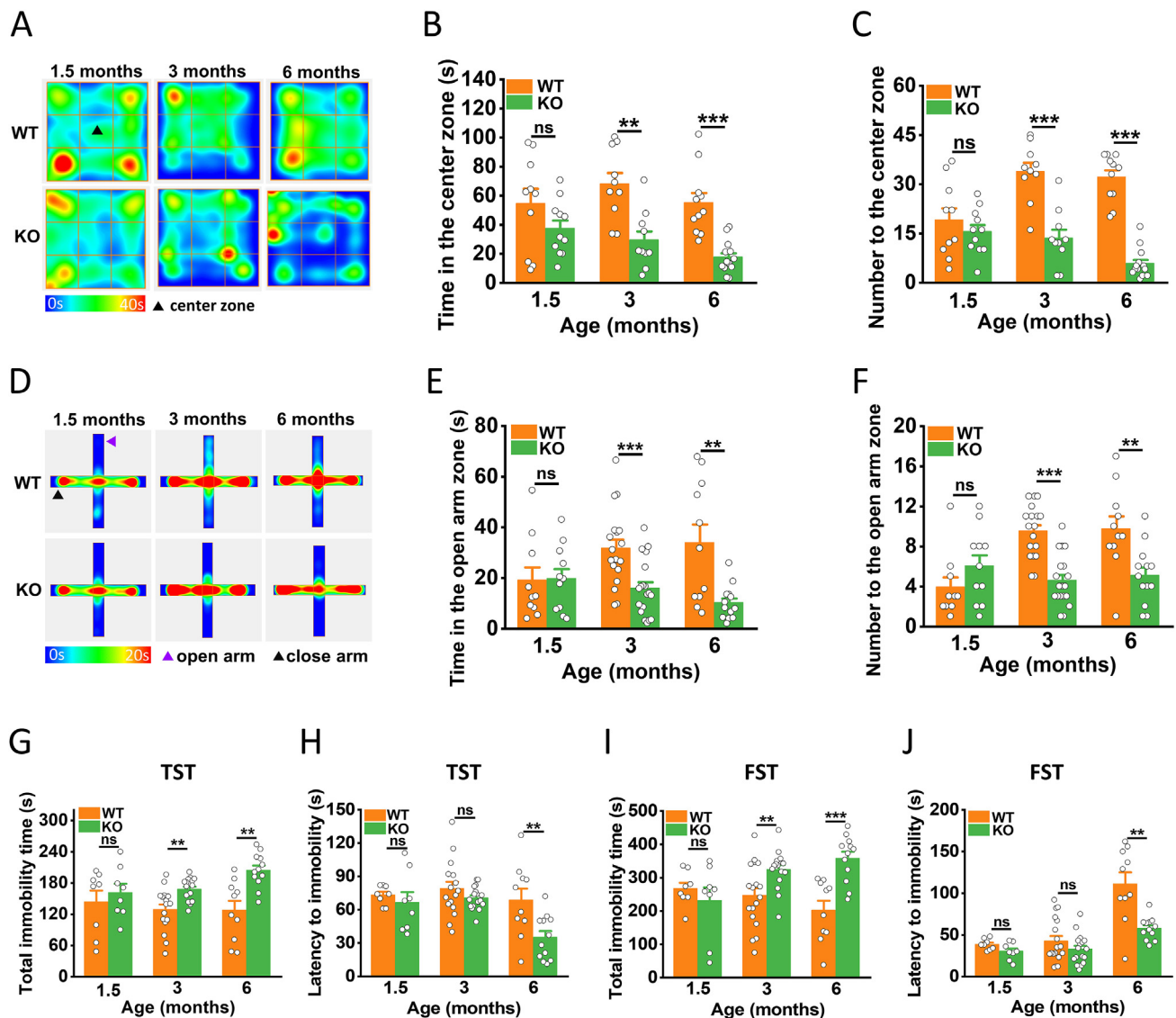
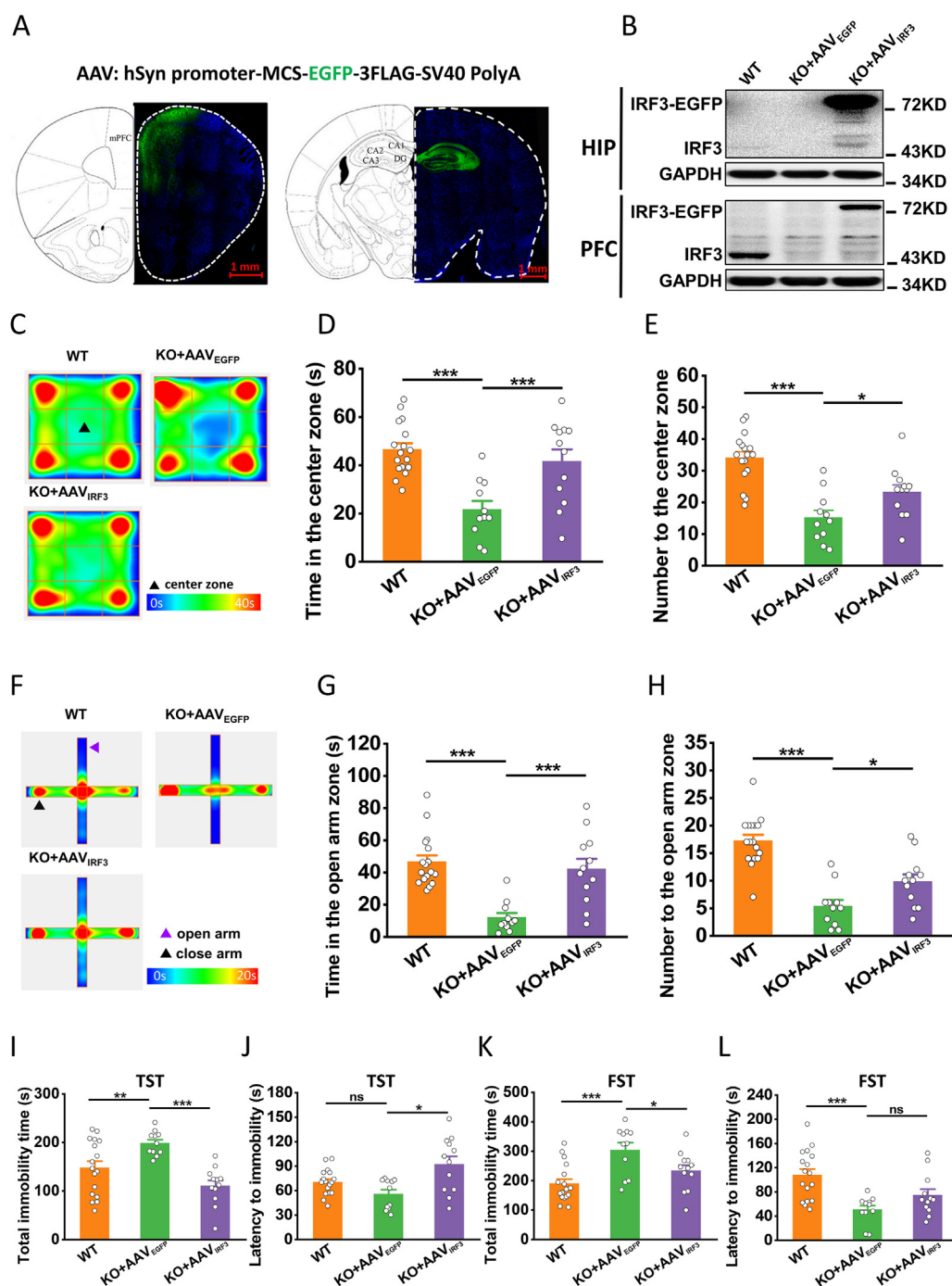


**Figure 2** *IRF3*-KO mice exhibit age-dependent anxiety/depression-like behaviors. (A) Representative heat maps in the open field test. (B) The time spent in the center zone during the open field test ( $n = 10$ – $13$  per group). Unpaired Student's  $t$ -test: 1.5 m,  $t = 3.537$ ,  $P = 0.159$ ; 3 m,  $t = 0.498$ ,  $P = 0.001$ ; 6 m,  $t = 3.756$ ,  $P < 0.001$ . (C) The number of entries in the center zone during the open field test. Unpaired Student's  $t$ -test: 1.5 m,  $t = 4.468$ ,  $P = 0.416$ ; 3 m,  $t = 0.001$ ,  $P < 0.001$ ; 6 m,  $t = 4.797$ ,  $P < 0.001$ . (D) Representative heat maps in the elevated plus maze test. (E) The time spent in the open arm during the elevated plus maze test ( $n = 10$ – $19$  per group). Unpaired Student's  $t$ -test: 1.5 m,  $t = 0.584$ ,  $P = 0.921$ ; 3 m,  $t = 1.281$ ,  $P < 0.001$ ; 6 m,  $t = 30.364$ ,  $P = 0.009$ . (F) The number of entries to the open arm during the elevated plus maze test. Unpaired Student's  $t$ -test: 1.5 m,  $t = 0.919$ ,  $P = 0.184$ ; 3 m,  $t = 0.172$ ,  $P < 0.001$ ; 6 m,  $t = 0.602$ ,  $P = 0.004$ . (G) The total immobility time in tail suspension test (TST) ( $n = 8$ – $17$  per group). Unpaired Student's  $t$ -test: 1.5 m,  $t = 1.601$ ,  $P = 0.535$ ; 3 m,  $t = 5.315$ ,  $P = 0.003$ ; 6 m,  $t = 5.876$ ,  $P = 0.002$ . (H) The latency to immobility in TST. Unpaired Student's  $t$ -test: 1.5 m,  $t = 6.421$ ,  $P = 0.512$ ; 3 m,  $t = 6.714$ ,  $P = 0.241$ ; 6 m,  $t = 2.690$ ,  $P = 0.008$ . (I) The total immobility time in forced swimming test (FST) ( $n = 8$ – $17$  per group). Unpaired Student's  $t$ -test: 1.5 m,  $t = 3.454$ ,  $P = 0.429$ ; 3 m,  $t = 4.967$ ,  $P = 0.007$ ; 6 m,  $t = 2.017$ ,  $P < 0.001$ . (J) The latency to immobility in FST. Unpaired Student's  $t$ -test: 1.5 m,  $t = 1.148$ ,  $P = 0.074$ ; 3 m,  $t = 4.296$ ,  $P = 0.267$ ; 6 m,  $t = 12.528$ ,  $P = 0.004$ . Data are expressed as mean  $\pm$  SEM. \* $P < 0.05$ , \*\* $P < 0.01$ , \*\*\* $P < 0.001$ ; ns, no significant difference.

(KO + AAV<sub>EGFP</sub>,  $P < 0.001$  vs. WT; KO + AAV<sub>IRF3</sub>,  $P = 0.021$  vs. KO + AAV<sub>EGFP</sub>; Fig. 3C, E) into the center zone during the open field test in *IRF3*-KO mice infected with AAV<sub>IRF3</sub>, but not its control AAV<sub>EGFP</sub>. During the elevated plus maze test, the *IRF3*-KO mice infected with AAV<sub>IRF3</sub> exhibited a significant increase in time (WT,  $n = 17$ ; KO + AAV<sub>EGFP</sub>,  $n = 11$ ,  $P < 0.001$  vs. WT; KO + AAV<sub>IRF3</sub>,  $n = 12$ ,  $P < 0.001$  vs.

KO + AAV<sub>EGFP</sub>; Fig. 3F, G) and number of entries in the open arm (KO + AAV<sub>EGFP</sub>,  $P < 0.001$  vs. WT; KO + AAV<sub>IRF3</sub>,  $P = 0.019$  vs. KO + AAV<sub>EGFP</sub>; Fig. 3F, H).

During tail suspension test, the *IRF3*-KO mice infected with AAV<sub>IRF3</sub>, but not AAV<sub>EGFP</sub>, displayed reduced total immobility time (WT,  $n = 17$ ; KO + AAV<sub>EGFP</sub>,  $n = 11$ ,  $P = 0.007$  vs. WT; KO + AAV<sub>IRF3</sub>,  $n = 12$ ,  $P < 0.001$  vs.



KO + AAV<sub>EGFP</sub>; Fig. 3I) and increased latency to immobility (KO + AAV<sub>EGFP</sub>,  $P = 0.132$  vs. WT; KO + AAV<sub>IRF3</sub>,  $n = 12$ ,  $P = 0.014$  vs. KO + AAV<sub>EGFP</sub>; Fig. 3J). Similar to that in the tail suspension test, AAV<sub>IRF3</sub> microinjection, but not AAV<sub>EGFP</sub>, significantly reduced the total immobility time (WT,  $n = 17$ ; KO + AAV<sub>EGFP</sub>,  $n = 11$ ,  $P < 0.001$  vs. WT; KO + AAV<sub>IRF3</sub>,  $n = 12$ ,  $P = 0.022$  vs. KO + AAV<sub>EGFP</sub>; Fig. 3K), although the latency to immobility remained unchanged (KO + AAV<sub>EGFP</sub>,  $P < 0.001$  vs. WT; KO + AAV<sub>IRF3</sub>,  $n = 12$ ,  $P = 0.112$  vs. KO + AAV<sub>EGFP</sub>; Fig. 3L) during forced swimming test. Taken together, these findings suggest that restoring IRF3 expression in the brain of IRF3-KO mice effectively relieves anxiety/depression-like behaviors.

### IRF3 deficiency results in hyperexcitability of mPFC neurons

Previous studies have shown that emotional disorders like anxiety and depression are usually associated with an imbalance of the excitatory/inhibitory (E/I) in the mPFC.<sup>8,42,43</sup> Since IRF3-KO mice display increased anxiety/depression-like behaviors, we hypothesized a lack of IRF3 will affect E/I balance in the mPFC. The electrophysiological properties including action potentials (APs), miniature excitatory postsynaptic currents (mEPSCs) and miniature inhibitory postsynaptic currents (mIPSCs) of neurons were examined in acute mPFC slices from IRF3-KO mice infected with AAV<sub>IRF3</sub> or AAV<sub>EGFP</sub>. We recorded the mPFC neurons that were expressing fluorescently identifiable IRF3 (Green) (Fig. 3A, left). The results showed that the resting membrane potential (RMP) remained unchanged in IRF3-KO mice infected with AAV<sub>IRF3</sub> or AAV<sub>EGFP</sub>, compared to WT (WT,  $n = 15$ ; KO + AAV<sub>EGFP</sub>,  $n = 18$ ,  $P = 0.818$  vs. WT; KO + AAV<sub>IRF3</sub>,  $n = 16$ ,  $P = 0.260$  vs. KO + AAV<sub>EGFP</sub>; Fig. 4B). Notably, the mPFC neurons from IRF3-KO mice infected with AAV<sub>EGFP</sub> displayed lower threshold ( $P = 0.017$  vs. WT; Fig. 4C) and higher firing frequency ( $P = 0.005$  vs. WT; Fig. 4A, D) of APs, compared to WT. As expected, AAV<sub>IRF3</sub> infection restored the threshold ( $P = 0.964$  vs. WT,  $P = 0.021$  vs. KO + AAV<sub>EGFP</sub>; Fig. 4C) and firing frequency ( $P = 0.508$  vs. WT,  $P = 0.038$  vs. KO + AAV<sub>EGFP</sub>; Fig. 4A, D) of APs to WT level.

The results from mEPSC recordings showed that AAV<sub>EGFP</sub> infection dramatically increased the amplitude (WT,  $n = 19$ ; KO + AAV<sub>EGFP</sub>,  $n = 23$ ,  $P < 0.001$  vs. WT; Fig. 4E, F) and frequency ( $P < 0.001$  vs. WT; Fig. 4E, G) of mEPSC, in comparison with their WT counterparts. The amplitude (KO + AAV<sub>IRF3</sub>,  $n = 22$ ,  $P = 0.525$  vs. WT,  $P = 0.001$  vs. KO + AAV<sub>EGFP</sub>; Fig. 4E, F) and frequency ( $P = 0.384$  vs. WT,  $P < 0.001$  vs. KO + AAV<sub>EGFP</sub>; Fig. 4E, G) of mEPSCs were fully restored in neurons overexpressing AAV<sub>IRF3</sub> in IRF3-KO mice. Further mIPSC recordings showed that both mIPSC amplitude (WT,  $n = 19$ ; KO + AAV<sub>EGFP</sub>,  $n = 18$ ,  $P < 0.001$  vs. WT; Fig. 4H, I) and frequency ( $P < 0.001$  vs. WT; Fig. 4H, J) were decreased in IRF3-KO mice infected with AAV<sub>EGFP</sub>, compared to WT. Similar to that in mEPSC recordings, mPFC neurons overexpressing AAV<sub>IRF3</sub> fully restored the mIPSC amplitude (KO + AAV<sub>IRF3</sub>,  $n = 17$ ,  $P = 0.503$  vs. WT,  $P < 0.001$  vs. KO + AAV<sub>EGFP</sub>; Fig. 4H, I) and frequency ( $P = 0.703$  vs. WT,  $P < 0.001$  vs. KO + AAV<sub>EGFP</sub>; Fig. 4H, J) in IRF3-KO mice. Collectively, these results described here

support the assertion that IRF3 ablation results in hyperexcitability of mPFC neurons, and that the hyperexcitability can be suppressed by restoring the expression of IRF3.

### IRF3 deficiency results in hyperexcitability of hippocampal CA1 neurons

Similar to the prefrontal cortex, the hippocampus is also a key region for emotional control.<sup>10,44</sup> Therefore, we next examined the E/I balance in the hippocampal CA1 pyramidal neurons overexpressing IRF3 from IRF3-KO mice (Fig. 3A, right). As shown in Figure 5A–D, all APs properties including the RMP (WT,  $n = 17$ ; KO + AAV<sub>EGFP</sub>,  $n = 22$ ,  $P = 0.917$  vs. WT; KO + AAV<sub>IRF3</sub>,  $n = 20$ ,  $P = 0.857$  vs. KO + AAV<sub>EGFP</sub>; Fig. 5B), threshold (KO + AAV<sub>EGFP</sub>,  $P = 0.590$  vs. WT; KO + AAV<sub>IRF3</sub>,  $P = 0.627$  vs. WT,  $P = 0.964$  vs. KO + AAV<sub>EGFP</sub>; Fig. 5C) and firing frequency (KO + AAV<sub>EGFP</sub>,  $P = 0.901$  vs. WT; KO + AAV<sub>IRF3</sub>,  $P = 0.841$  vs. WT,  $P = 0.933$  vs. KO + AAV<sub>EGFP</sub>; Fig. 5A, D) were unaltered in hippocampal CA1 neurons from IRF3-KO mice infected with either AAV<sub>EGFP</sub> or AAV<sub>IRF3</sub>, compared to WT. However, both the amplitude (WT,  $n = 15$ ; KO + AAV<sub>EGFP</sub>,  $n = 14$ ,  $P < 0.001$  vs. WT; Fig. 5E, F) and frequency ( $P = 0.042$  vs. WT; Fig. 5E, G) of mEPSCs were increased in the hippocampal CA1 pyramidal neurons from IRF3-KO mice infected with AAV<sub>EGFP</sub> compared to WT, while AAV<sub>IRF3</sub> microinjection significantly reversed the mEPSC amplitude (KO + AAV<sub>IRF3</sub>,  $n = 11$ ,  $P = 0.044$  vs. WT,  $P = 0.046$  vs. KO + AAV<sub>EGFP</sub>; Fig. 5E, F), although mEPSC frequency remained unchanged ( $P = 0.641$  vs. WT,  $P = 0.147$  vs. KO + AAV<sub>EGFP</sub>; Fig. 5E, G). Further mIPSC recordings showed that the amplitude (WT,  $n = 20$ ; KO + AAV<sub>EGFP</sub>,  $n = 18$ ,  $P = 0.001$  vs. WT; Fig. 5H, I), but not frequency ( $P = 0.155$  vs. WT; Fig. 5H, J), of mEPSCs were decreased in the hippocampal CA1 pyramidal neurons from IRF3-KO mice infected with AAV<sub>EGFP</sub> compared to WT, while AAV<sub>IRF3</sub> microinjection significantly reversed the mIPSC amplitude (KO + AAV<sub>IRF3</sub>,  $n = 21$ ,  $P = 0.718$  vs. WT,  $P < 0.001$  vs. KO + AAV<sub>EGFP</sub>; Fig. 5H, I) and frequency ( $P = 0.024$  vs. WT,  $P < 0.001$  vs. KO + AAV<sub>EGFP</sub>; Fig. 5H, J). Taken together, our findings suggest that IRF3 deficiency also causes hyperexcitability of the hippocampal CA1 neurons, and that restoring IRF3 expression partially reverses these changes.

## Discussion

IRF3 is a key transcription factor for anti-infection response and regulating type I IFN expression.<sup>22,23</sup> Increasing evidence suggests that IRF3 mutation or abnormal expression may contribute to neurological or psychiatric disorders, such as schizophrenia<sup>45</sup> and stroke.<sup>27,28</sup> Importantly, clinical studies have shown that the transcription level of IRF3 is reduced in blood in patients with early-onset depression and anxiety comorbid disorders caused by chronic stress.<sup>41</sup> Similarly, studies in animal models have shown that under conditions of chronic restraint stress (CRS), transcriptional levels of IRF3 in the hippocampus are reduced even when IRF3 levels in the blood do not change.<sup>46</sup> Based on these studies, it appears that IRF3 plays an important role in depression comorbid with anxiety disorders, or in simple depression, although the mechanism remains unclear.

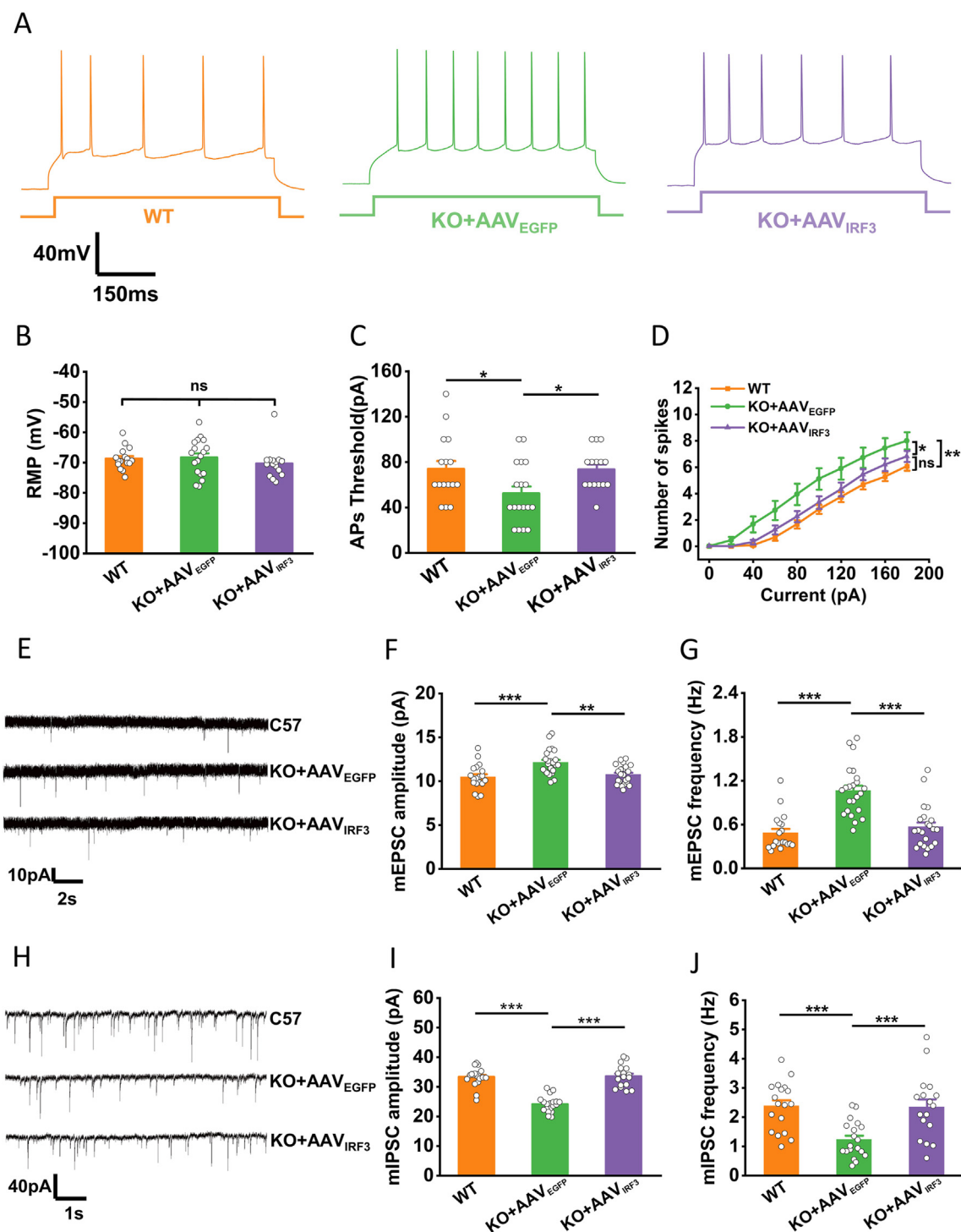


**Figure 4** *IRF3*-KO results in neuronal hyperexcitability in the mPFC. **(A)** Representative AP firing in the mPFC neurons. **(B)** Bar graphs of the resting membrane potential (RMP) in mPFC neurons ( $n = 15\text{--}18$  cells from 3 mice per group). One-way ANOVA:  $F(2,46) = 19.412$ ,  $P = 0.498$ . **(C)** Bar graphs of the APs threshold in mPFC neurons. One-way ANOVA:  $F(2,46) = 4.708$ ,  $P = 0.023$ . **(D)** Bar graphs of the number of APs evoked by current injections from 0 to 180 pA. Repeated measures ANOVA:  $F(2,46) = 186.142$ ,  $P = 0.020$ . **(E)** Representative mEPSC traces in the mPFC neurons. **(F)** Bar graphs of mEPSCs amplitude ( $n = 19\text{--}23$  cells from 3 mice per group). One-way ANOVA:  $F(2,61) = 9.997$ ,  $P < 0.001$ . **(G)** Bar graphs of mEPSCs frequency. One-way ANOVA:  $F(2,61) = 23.620$ ,  $P < 0.001$ . **(H)** Representative mIPSCs traces in the mPFC neurons. **(I)** Bar graphs of mIPSCs amplitude ( $n = 17\text{--}19$  cells from 3 to 4 mice per group). One-way ANOVA:  $F(2,52) = 41.788$ ,  $P < 0.001$ . **(J)** Bar graphs of mIPSCs frequency. One-way ANOVA:  $F(2,52) = 11.195$ ,  $P < 0.001$ . Data are expressed as mean  $\pm$  SEM, \* $P < 0.05$ , \*\* $P < 0.01$ , \*\*\* $P < 0.001$ ; ns, no significant difference.

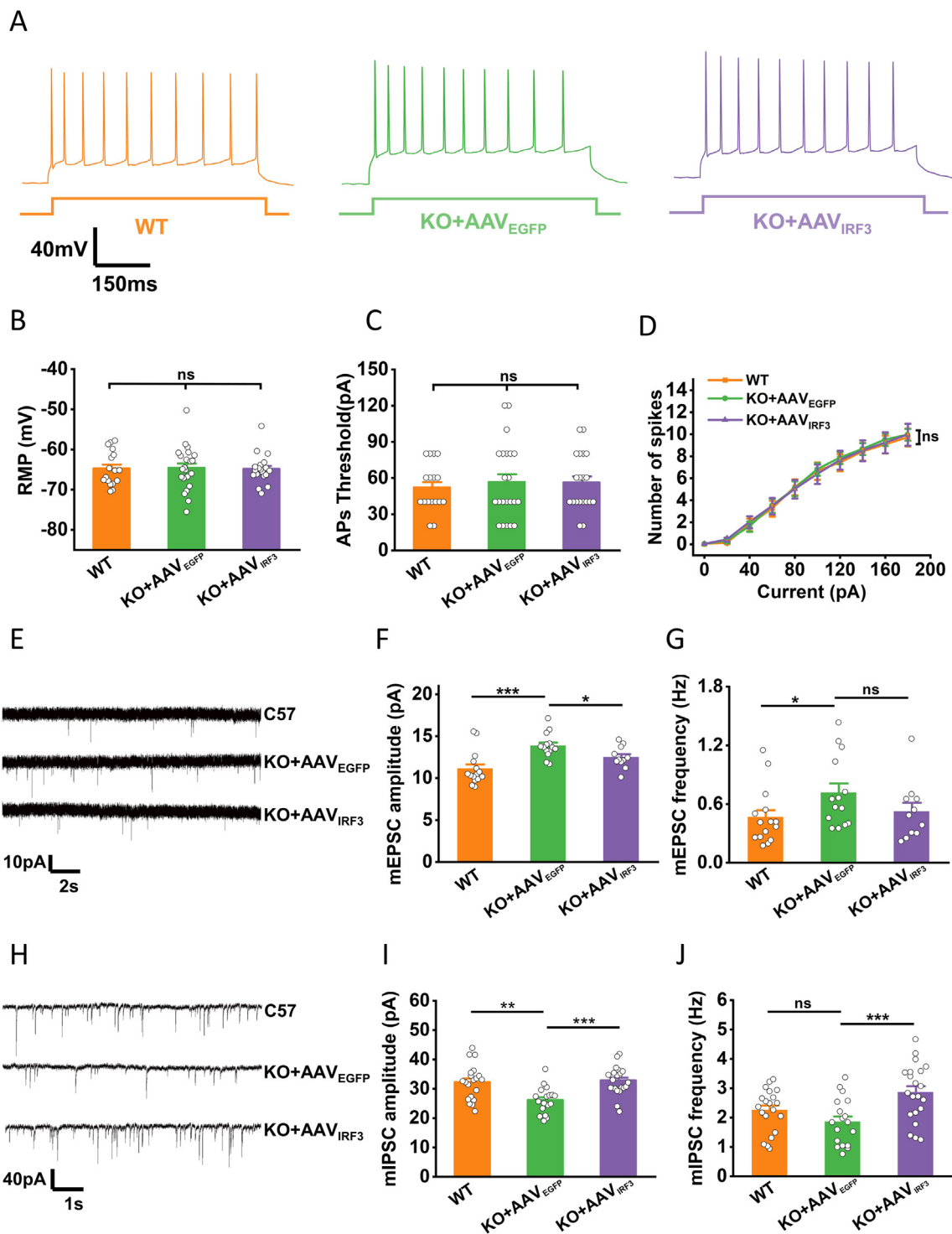


**Figure 5** *IRF3*-KO results in neuronal hyperexcitability in the CA1 area of the hippocampus. (A) Representative AP firing in the hippocampal CA1 neurons. (B) Bar graphs of the RMP in the hippocampal CA1 neurons ( $n = 17-22$  cells from 3 mice per group). One-way ANOVA:  $F(2,56) = 0.017$ ,  $P = 0.983$ . (C) Bar graphs of the APs threshold. One-way ANOVA:  $F(2,56) = 0.173$ ,  $P = 0.842$ . (D) Bar graphs of the number of APs evoked by current injections from 0 to 180 pA. Repeated measures ANOVA:  $F(2,56) = 254.068$ ,  $P = 0.980$ . (E) Representative mEPSCs traces of the hippocampal CA1 neurons. (F) Bar graphs of mEPSCs amplitude ( $n = 11-15$  cells from 3 to 4 mice per group). One-way ANOVA:  $F(2,37) = 9.976$ ,  $P < 0.001$ . (G) Bar graphs of mEPSCs frequency. One-way ANOVA:  $F(2,37) = 2.372$ ,  $P = 0.107$ . (H) Representative mIPSCs traces of the hippocampal CA1 neurons. (I) mIPSCs amplitude of CA1 neurons ( $n = 18-21$  cells from 3 mice per group). One-way ANOVA:  $F(2,56) = 9.772$ ,  $P < 0.001$ . (J) Bar graphs of mIPSCs frequency. One-way ANOVA:  $F(2,56) = 7.089$ ,  $P = 0.002$ . Data are expressed as mean  $\pm$  SEM, \* $P < 0.05$ , \*\* $P < 0.01$ , \*\*\* $P < 0.001$ ; ns, no significant difference.

Consistent with these reports, we here found that *IRF3*-KO mice exhibited obvious anxiety/depression-like behaviors at 3–6 months of age (Fig. 2). Restoring *IRF3* expression in the brain by AAV microinjection almost completely rescued anxiety/depression-like behaviors in *IRF3*-KO mice (Fig. 3), suggesting that maintaining the expression of *IRF3* in the brain is indeed critical for emotional stability. However, these findings are challenged by a recent study showing that Silibinin can alleviate anxiety and depression in the MPTP mice model of Parkinson's disease through suppressing *IRF3* pathway.<sup>47</sup> A possible explanation is that *IRF3* has different roles in pathological and physiological conditions, and it may act as an inflammatory factor rather than a mood stabilizer in PD. Notably, although anxiety and depression can occur at all ages,<sup>48,49</sup> *IRF3*-KO mice did not display any anxiety/depression-like behaviors at 1.5-month old (adolescents), indicating that depression and comorbid anxiety disorders may be age-dependent in *IRF3*-deficient mice. Indeed, recent study has revealed that age-dependent transcriptional responses are observed following stroke, most of which involve inflammatory and immune responses, leading to a distinct age-related susceptibility for post-ischemic depression.<sup>50</sup>

It has been reported that mice lacking *IFN- $\beta$*  will suffer from cognitive deficits.<sup>51</sup> *IRF3* acts as a key upstream regulator of *IFN- $\beta$* ,<sup>52–54</sup> and may also affect learning and memory. However, we did not observe any spatial learning and memory deficits in *IRF3*-KO mice from adolescents (1.5 months) to adults (6 months) in the present study (Fig. 1). One possibility is that *IFN- $\beta$*  may be also regulated by other molecules, such as *IRF1*,<sup>55</sup> so that mice lacking *IRF3* do not display cognitive problems associated with *IFN- $\beta$*  deficiency. Alternatively, *IRF3* deficiency may affect other types of learning and memory, such as working memory, rather than spatial learning memory. Thus, the expression of *IFN- $\beta$*  and other types of learning and memory need to be further studied in *IRF3*-deficient mice in the future.

Many previous studies have reported that the E/I balance plays critical roles in normal brain functions.<sup>6,7</sup> In the mammalian central nervous system, the E/I balance is maintained by synaptic excitation mediated by the principle excitatory transmitter glutamate and synaptic inhibition mediated by inhibitory transmitter  $\gamma$ -aminobutyric acid (GABA). A growing body of evidence is showing that disruption of the E/I balance may cause neuropsychiatric disorders, including anxiety and depression.<sup>10</sup> For example, previous study has shown that GABA<sub>A</sub> receptor  $\gamma 2$  subunit heterozygous ( $\gamma 2^{+/-}$ ) mice can be used as major depressive disorder model.<sup>56</sup> Ketamine, as a classic antidepressant, can inhibit the NMDAR-dependent burst firing, thereby normalizing neuronal excitability in the lateral habenula in rat and mouse models of depression.<sup>57,58</sup> In addition, clinical studies suggest that tiagabine could treat anxiety and comorbid depressive symptoms by enhancing GABA neurotransmission.<sup>59</sup> These findings indicate that simple depression or comorbidities of anxiety and depression may be characterized by reduced GABAergic transmission and/or increased glutamatergic transmission. Consistent with these findings, we here reported that *IRF3* deficiency significantly increased neuronal excitation and reduced inhibition in the mPFC and hippocampal CA1 area (Fig. 4,

5), two key regions for anxiety and depression.<sup>11,12</sup> More importantly, restoring *IRF3* expression in the neurons of mPFC and hippocampal CA1 by AAV microinjection fully reversed the E/I imbalance to physiological level (Fig. 4, 5), thereby alleviating anxiety/depression-like behaviors (Fig. 3) in *IRF3*-KO mice. Thus, these findings indicate that *IRF3* plays an important role in maintaining neuronal E/I balance and emotional stability. Notably, E/I imbalance caused by *IRF3* deficiency did not affect spatial learning and memory (Fig. 1) in the present study, which is contrary to previous reports that neuronal hyperactivity is parallel to the impairment of cognitive functions in epilepsy.<sup>60</sup> One possible explanation is that many other factors, such as cell death and synaptic reorganization, contribute to cognitive impairment in epilepsy besides E/I imbalance. In addition, although we detected E/I balance in the present study, further molecular mechanism underlying anxiety and depression in *IRF3*-KO mice is not clear. Therefore, further studies including detection of the expression of excitatory and inhibitory receptors in the mPFC and hippocampal CA1, and whether *IRF3* interacts with these receptors need to be conducted in the future.

In summary, we present the first evidence that knockout of *IRF3* can significantly affect the neuronal excitability in the mPFC and hippocampal CA1 area, thereby leading to an age-dependent anxiety-depression coexistence phenotype. We further demonstrate that rescue of *IRF3* expression by microinjection of AAV carrying functional *IRF3* successfully restores behavior and electrophysiology to physiological levels. Taken together, these findings suggest that *IRF3* may act as a mood stabilizer in the brain and potentially as a novel molecule for the treatment of mood disorders.

## Author contributions

JL and ZD conceived the study. JL, YD and ZD wrote the manuscript. JL performed behavioral tests. JL, MC and YF performed biochemical assay. JL and YP performed electrophysiological experiments. JL, YD, and LX analyzed the data.

## Conflict of interests

The authors have declared that no conflict of interest exists.

## Funding

This work was supported by grants from the National Natural Science Foundation of China (No. 82071395 and 82001158), the Natural Science Foundation of Chongqing, China (No. cstc2021ycjh-bgzxm0186 and cstc2020jcyj-zdxmX0004), the Science and Technology Research Program of Chongqing Municipal Education Commission, China (No. KJZD-K201900403), Innovation Research Group at Institutions of Higher Education in Chongqing, China (No. CXQTP19034) and CQMU Program for Youth Innovation in Future Medicine, China (No. W0044).

## Acknowledgements

We thank Professor Sen Lin (Army Medical University, Chongqing, China) for kindly providing *IRF3*<sup>-/-</sup> mice. We are also grateful to other members in the Dong laboratory for the technical support and helpful suggestion.

## References

- Charlson F, van Ommeren M, Flaxman A, et al. New WHO prevalence estimates of mental disorders in conflict settings: a systematic review and meta-analysis. *Lancet*. 2019; 394(10194):240–248.
- Huang Y, Wang Y, Wang H, et al. Prevalence of mental disorders in China: a cross-sectional epidemiological study. *Lancet Psychiatry*. 2019;6(3):211–224.
- Cosci F, Fava GA. When anxiety and depression coexist: the role of differential diagnosis using clinimetric criteria. *Psychother Psychosom*. 2021;90(5):308–317.
- Coplan JD, Aaronson CJ, Panthangi V, et al. Treating comorbid anxiety and depression: psychosocial and pharmacological approaches. *World J Psychiatry*. 2015;5(4):366–378.
- Spijker J, Muntingh A, Batelaan N. Advice for clinicians on how to treat comorbid anxiety and depression. *JAMA Psychiatry*. 2020;77(6):645–646.
- Sohal VS, Rubenstein JLR. Excitation-inhibition balance as a framework for investigating mechanisms in neuropsychiatric disorders. *Mol Psychiatry*. 2019;24(9):1248–1257.
- He HY, Shen W, Zheng L, et al. Excitatory synaptic dysfunction cell-autonomously decreases inhibitory inputs and disrupts structural and functional plasticity. *Nat Commun*. 2018;9(1):2893.
- Page CE, Coutellier L. Prefrontal excitatory/inhibitory balance in stress and emotional disorders: evidence for over-inhibition. *Neurosci Biobehav Rev*. 2019;105:39–51.
- Tatti R, Haley MS, Swanson OK, et al. Neurophysiology and regulation of the balance between excitation and inhibition in neocortical circuits. *Biol Psychiatry*. 2017;81(10):821–831.
- Fogaça MV, Duman RS. Cortical GABAergic dysfunction in stress and depression: new insights for therapeutic interventions. *Front Cell Neurosci*. 2019;13:87.
- Godsil BP, Kiss JP, Spedding M, et al. The hippocampal-prefrontal pathway: the weak link in psychiatric disorders? *Eur Neuropsychopharmacol*. 2013;23(10):1165–1181.
- Sigurdsson T, Duvarci S. Hippocampal-prefrontal interactions in cognition, behavior and psychiatric disease. *Front Syst Neurosci*. 2016;9:190.
- Quidé Y, Witteveen AB, El-Hage W, et al. Differences between effects of psychological versus pharmacological treatments on functional and morphological brain alterations in anxiety disorders and major depressive disorder: a systematic review. *Neurosci Biobehav Rev*. 2012;36(1):626–644.
- Nguyen H, Hiscott J, Pitha PM. The growing family of interferon regulatory factors. *Cytokine Growth Factor Rev*. 1997;8(4):293–312.
- Hiscott J, Pitha P, Genin P, et al. Triggering the interferon response: the role of IRF-3 transcription factor. *J Interferon Cytokine Res*. 1999;19(1):1–13.
- Doyle S, Vaidya S, O'Connell R, et al. IRF3 mediates a TLR3/TLR4-specific antiviral gene program. *Immunity*. 2002; 17(3):251–263.
- Antonczyk A, Krist B, Sajek M, et al. Direct inhibition of IRF-dependent transcriptional regulatory mechanisms associated with disease. *Front Immunol*. 2019;10:1176.
- Petro TM. IFN regulatory factor 3 in health and disease. *J Immunol*. 2020;205(8):1981–1989.
- Tarassishin L, Bauman A, Suh HS, et al. Anti-viral and anti-inflammatory mechanisms of the innate immune transcription factor interferon regulatory factor 3: relevance to human CNS diseases. *J Neuroimmune Pharmacol*. 2013;8(1):132–144.
- Cai Z, Zhang MX, Tang Z, et al. USP22 promotes IRF3 nuclear translocation and antiviral responses by deubiquitinating the importin protein KPNA2. *J Exp Med*. 2020;217(5):e20191174.
- Lei CQ, Zhong B, Zhang Y, et al. Glycogen synthase kinase 3 $\beta$  regulates IRF3 transcription factor-mediated antiviral response via activation of the kinase TBK1. *Immunity*. 2010;33(6):878–889.
- Tsuchida T, Kawai T, Akira S. Inhibition of IRF3-dependent antiviral responses by cellular and viral proteins. *Cell Res*. 2009;19(1):3–4.
- Wang C, Wang Q, Xu X, et al. The methyltransferase NSD3 promotes antiviral innate immunity via direct lysine methylation of IRF3. *J Exp Med*. 2017;214(12):3597–3610.
- Brown MC, Mosaheb MM, Mohme M, et al. Viral infection of cells within the tumor microenvironment mediates antitumor immunotherapy via selective TBK1-IRF3 signaling. *Nat Commun*. 2021;12(1):1858.
- Jiao S, Guan J, Chen M, et al. Targeting IRF3 as a YAP agonist therapy against gastric cancer. *J Exp Med*. 2018;215(2):699–718.
- Tian M, Wang X, Sun J, et al. IRF3 prevents colorectal tumorigenesis via inhibiting the nuclear translocation of  $\beta$ -catenin. *Nat Commun*. 2020;11(1):5762.
- Li L, Qin JJ, Guo S, et al. Attenuation of cerebral ischemic injury in interferon regulatory factor 3-deficient rat. *J Neurochem*. 2016;136(4):871–883.
- Marsh B, Stevens SL, Packard AEB, et al. Systemic lipopolysaccharide protects the brain from ischemic injury by reprogramming the response of the brain to stroke: a critical role for IRF3. *J Neurosci*. 2009;29(31):9839–9849.
- Ahmad R, Al-Roub A, Kochumon S, et al. The synergy between palmitate and TNF- $\alpha$  for CCL2 production is dependent on the TRIF/IRF3 pathway: implications for metabolic inflammation. *J Immunol*. 2018;200(10):3599–3611.
- Kumari M, Wang X, Lantier L, et al. IRF3 promotes adipose inflammation and insulin resistance and represses browning. *J Clin Invest*. 2016;126(8):2839–2854.
- Tang P, Virtue S, Goie JYG, et al. Regulation of adipogenic differentiation and adipose tissue inflammation by interferon regulatory factor 3. *Cell Death Differ*. 2021;28(11):3022–3035.
- Wang XA, Zhang R, She ZG, et al. Interferon regulatory factor 3 constrains IKK $\beta$ /NF- $\kappa$ B signaling to alleviate hepatic steatosis and insulin resistance. *Hepatology*. 2014;59(3):870–885.
- Kostoula C, Shaker T, Cerovic M, et al. TLR3 preconditioning induces anti-inflammatory and anti-ictogenic effects in mice mediated by the IRF3/IFN- $\beta$  axis. *Brain Behav Immun*. 2019;81:598–607.
- Zhang X, Zhu J, Chen X, et al. Interferon regulatory factor 3 deficiency induces age-related alterations of the retina in young and old mice. *Front Cell Neurosci*. 2019;13:272.
- Xia L, Pang Y, Li J, et al. Dihydroartemisinin induces O-GlcNAcylation and improves cognitive function in a mouse model of tauopathy. *J Alzheimers Dis*. 2021;84(1):239–248.
- Chen L, Huang Z, Du Y, et al. Capsaicin attenuates amyloid- $\beta$ -induced synapse loss and cognitive impairments in mice. *J Alzheimers Dis*. 2017;59(2):683–694.
- Du Y, Fu M, Huang Z, et al. TRPV1 activation alleviates cognitive and synaptic plasticity impairments through inhibiting

- AMPA endocytosis in APP23/PS45 mouse model of Alzheimer's disease. *Aging Cell*. 2020;19(3):e13113.
38. Du Y, Du Y, Zhang Y, et al. MKP-1 reduces A $\beta$  generation and alleviates cognitive impairments in Alzheimer's disease models. *Signal Transduct Target Ther*. 2019;4:58.
  39. Wang W, Tan T, Tu M, et al. Acute pentobarbital treatment impairs spatial learning and memory and hippocampal long-term potentiation in rats. *Physiol Behav*. 2015;149:169–173.
  40. Kawai T, Morita K, Masuda K, et al. Gene expression signature in peripheral blood cells from medical students exposed to chronic psychological stress. *Biol Psychol*. 2007;76(3):147–155.
  41. Pajer K, Andrus BM, Gardner W, et al. Discovery of blood transcriptomic markers for depression in animal models and pilot validation in subjects with early-onset major depression. *Transl Psychiatry*. 2012;2(4):e101.
  42. Krystal JH, Sanacora G, Blumberg H, et al. Glutamate and GABA systems as targets for novel antidepressant and mood-stabilizing treatments. *Mol Psychiatry*. 2002;7 Suppl 1: S71–S80.
  43. Yin YY, Wang YH, Liu WG, et al. The role of the excitation: inhibition functional balance in the mPFC in the onset of antidepressants. *Neuropharmacology*. 2021;191:108573.
  44. Li YF. A hypothesis of monoamine (5-HT) - glutamate/GABA long neural circuit: aiming for fast-onset antidepressant discovery. *Pharmacol Ther*. 2020;208:107494.
  45. Li X, Zhang W, Lencz T, et al. Common variants of IRF3 conferring risk of schizophrenia. *J Psychiatr Res*. 2015;64: 67–73.
  46. Mehta-Raghavan NS, Wert SL, Morley C, et al. Nature and nurture: environmental influences on a genetic rat model of depression. *Transl Psychiatry*. 2016;6:e770.
  47. Liu X, Chen W, Wang C, et al. Silibinin ameliorates depression/anxiety-like behaviors of Parkinson's disease mouse model and is associated with attenuated STING-IRF3-IFN- $\beta$  pathway activation and neuroinflammation. *Physiol Behav*. 2021;241: 113593.
  48. Christensen H, Jorm AF, Mackinnon AJ, et al. Age differences in depression and anxiety symptoms: a structural equation modelling analysis of data from a general population sample. *Psychol Med*. 1999;29(2):325–339.
  49. Ghandour RM, Sherman LJ, Vladutiu CJ, et al. Prevalence and treatment of depression, anxiety, and conduct problems in US children. *J Pediatr*. 2019;206:256–267.
  50. Sieber MW, Guenther M, Jaenisch N, et al. Age-specific transcriptional response to stroke. *Neurobiol Aging*. 2014;35(7): 1744–1754.
  51. Ejlerskov P, Hultberg JG, Wang J, et al. Lack of neuronal IFN- $\beta$ -IFNAR causes Lewy body- and Parkinson's disease-like dementia. *Cell*. 2015;163(2):324–339.
  52. Escalante CR, Nistal-Villán E, Shen L, et al. Structure of IRF-3 bound to the PRDIII-I regulatory element of the human interferon-beta enhancer. *Mol Cell*. 2007;26(5):703–716.
  53. Honda K, Takaoka A, Taniguchi T. Type I interferon [corrected] gene induction by the interferon regulatory factor family of transcription factors. *Immunity*. 2006;25(3):349–360.
  54. Honda K, Taniguchi T. IRFs: master regulators of signalling by Toll-like receptors and cytosolic pattern-recognition receptors. *Nat Rev Immunol*. 2006;6(9):644–658.
  55. Yarilina A, Park-Min KH, Antoniv T, et al. TNF activates an IRF1-dependent autocrine loop leading to sustained expression of chemokines and STAT1-dependent type I interferon-response genes. *Nat Immunol*. 2008;9(4):378–387.
  56. Ren Z, Pribiag H, Jefferson SJ, et al. Bidirectional homeostatic regulation of a depression-related brain state by gamma-aminobutyric acidergic deficits and ketamine treatment. *Biol Psychiatry*. 2016;80(6):457–468.
  57. Yang Y, Cui Y, Sang K, et al. Ketamine blocks bursting in the lateral habenula to rapidly relieve depression. *Nature*. 2018; 554(7692):317–322.
  58. Shepard RD, Langlois LD, Browne CA, et al. Ketamine reverses lateral habenula neuronal dysfunction and behavioral immobility in the forced swim test following maternal deprivation in late adolescent rats. *Front Synaptic Neurosci*. 2018;10:39.
  59. Rosenthal M. Tiagabine for the treatment of generalized anxiety disorder: a randomized, open-label, clinical trial with paroxetine as a positive control. *J Clin Psychiatry*. 2003;64(10): 1245–1249.
  60. Holmes GL. Cognitive impairment in epilepsy: the role of network abnormalities. *Epileptic Disord*. 2015;17(2):101–116.